Geophysical Research Letters

RESEARCH LETTER
10.1029/2018GL081639

Quasi-Real-Time and High-Resolution Spatiotemporal Distribution of Ocean Anthropogenic CO_2

B. F. Li[1], Y. W. Watanabe[1], S. Hosoda[2], K. Sato[2], and Y. Nakano[3]

[1]Faculty of Environmental Earth Science, Hokkaido University, Sapporo, Japan, [2]Research Institute for Global Change, Global Ocean Observation Research Center, Global Oceanic Environment Research Group, Japan Agency for Marine-Earth Science and Technology, Yokosuka, Japan, [3]Institute for Marine-Earth Exploration and Engineering, Engineering Department, Marine Observational Engineering Group, Japan Agency for Marine-Earth Science and Technology, Yokosuka, Japan

Key Points:
- New parameterizations for total alkalinity and dissolved inorganic carbon allow higher-resolution estimates of oceanic anthropogenic CO_2
- Applying our parameterizations to autonomous biogeochemical Argo floats data could allow more detailed mapping of parameters influencing global oceanic CO_2 cycles

Supporting Information:
- Supporting Information S1
- Figure S1

Correspondence to:
B. F. Li,
mikolee@ees.hokudai.ac.jp

Citation:
Li, B. F., Watanabe, Y. W., Hosoda, S., Sato, K., & Nakano, Y. (2019). Quasi-real-time and high-resolution spatiotemporal distribution of ocean anthropogenic CO_2. *Geophysical Research Letters*, *46*, 4836–4843. https://doi.org/10.1029/2018GL081639

Received 12 DEC 2018
Accepted 3 APR 2019
Accepted article online 8 APR 2019
Published online 14 MAY 2019

Abstract Increasing marine uptake of anthropogenic CO_2 (C_{ant}) causes global ocean acidification. To obtain a high-resolution spatiotemporal distribution of oceanic carbon chemistry, we developed new parameterizations of the seawater total alkalinity, and dissolved inorganic carbon from the ocean's surface to 2,000-m depth by using dissolved oxygen, water temperature (T), salinity (S), and pressure (P) data. Using the values of total alkalinity and dissolved inorganic carbon predicted by dissolved oxygen, T, S, and P data derived from autonomous biogeochemical Argo floats, we described the distribution of oceanic C_{ant} in the 2000s in the subarctic North Pacific at high spatiotemporal resolution. The C_{ant} was found about 300 m deeper than during the 1990s; its average inventory to 2,000 m was 24.8 ± 10.2 mol/m^2, about 20% higher than the 1990s average. Future application of parameterizations to global biogeochemical Argo floats data should allow the detailed global mapping of spatiotemporal distributions of CO_2 parameters.

Plain Language Summary Ocean absorbs the increasing atmospheric CO_2 by human activities from 1750s and encourages global ocean acidification. To obtain the human-activity-derived CO_2 in the subarctic North Pacific in a high resolution, we applied our empirical ocean carbon chemistry equations using other hydrographic parameters to autonomous biogeochemical Argo floats data. The amount of human-activity-derived CO_2 in this region was found about 300 m deeper than during the 1990s and about 20% higher than the 1990s average. Our method allows the development of a system for monitoring long-term trend changes in ocean carbon chemistry similar to other time series stations.

1. Introduction

The global carbon cycle is of increasing interest due to the greenhouse effect of carbon dioxide (CO_2) on the Earth's climate. Since the 1750s, the ocean has played an important role as a sink of anthropogenic CO_2, absorbing almost one fourth of such emissions (Le Quere et al., 2014). Increasing marine CO_2 levels have mostly negatively impacted marine organisms by causing ocean acidification and reducing the ocean's buffering capacity (Doney et al., 2009).

To better understand changes in oceanic carbon chemistry, oceanographers have collected high-precision carbon chemistry data, including total alkalinity (TA), dissolved inorganic carbon (DIC), and pH within 0.1% precision, throughout the global ocean from the surface to the bottom waters at decadal-scale temporal resolutions since the last several decades of the twentieth century (Suzuki et al., 2013). However, such data were collected mainly during research cruises, limiting their value; ship-based data cannot provide information on annual, seasonal, or monthly variability, and their spatial resolution (distance between observation stations) tends to be only 2–5° of latitude and longitude (~100–500 km). Although time series data sets for long-term oceanic CO_2 variations from stationary observation sites are available in some representative regions (e.g., ocean stations ALOHA, Papa, and KNOT in the North Pacific; BATS in the North Atlantic), time series data sets across the global ocean are spatially sparse (e.g., the Carbon Dioxide Information Analysis Center: http://cdiac.ornl.gov/oceans).

To overcome these limitations and complement observed carbon chemistry data, researchers have developed parameterizations and models of oceanic CO_2 (Lee et al., 2006; Nakano & Watanabe, 2005; Williams et al., 2016). They use other hydrographical properties measured at higher spatial and temporal resolutions than carbon chemistry, including dissolved oxygen (DO), temperature (T), salinity (S), chlorophyll-a (Chl),

and nitrate (NO_3^-), to clarify spatiotemporal changes in oceanic carbon chemistry (Alin et al., 2012; Juranek et al., 2011; Li et al., 2016; Nakano & Watanabe, 2005; Takeshita et al., 2013).

Starting in 2000, researchers deployed an array of autonomous floats across the global ocean to monitor large and long-term oceanic changes as part of the Argo mission. These floats measure *T* and *S* from the sea surface to a depth of 2,000 m every 5–10 days (Carval et al., 2017). Over 3,000 Argo floats are now active and delivering real-time quality controlled data with high accuracy and horizontal/vertical resolutions, making it possible to analyze basin-scale oceanic changes more accurately than ever before. Furthermore, recently developed biogeochemical Argo floats (BGC-Argo) that can sense DO, NO_3^-, Chl, and more have been increasingly deployed (Johnson et al., 2017; Thierry & Bittig, 2016). Although the BGC-Argo project intends to develop a global array, only 8% of Argo floats currently have DO sensors (DO-Argo), and quality control is not yet complete due to complex procedures (Johnson et al., 2017; Takeshita et al., 2013; Thierry & Bittig, 2016). Thus, there is great potential for improved understanding of oceanic carbon chemistry processes when the current challenges are overcome although the use of DO-Argo data has so far been limited to some pilot studies of eddies, mixed layer depth and ocean circulation, and biological properties for net production (Bushinsky et al., 2017; Inoue & Kouketsu, 2015; Riser & Johnson, 2008; Takeshita et al., 2013).

To obtain an oceanic carbon chemistry data set with the same spatiotemporal scale as the high-resolution Argo physical and biological data sets, parameterization techniques have been applied to the Argo data sets (Juranek et al., 2011; Li et al., 2016; Williams et al., 2015). Simple, high-precision parameterizations of oceanic TA, DIC, and pH have previously been applied to DO, *T*, and *S* observational data collected by Argo floats in the subarctic North Pacific and used to produce quasi-real-time high-resolution maps of the vertical distributions of carbon chemistry to 400-m depth (Li et al., 2016). Moreover, the North Pacific Intermediate Water, a cold low-salinity mass produced in the western subarctic North Pacific, affects the climate and ocean circulation of the entire North Pacific (e.g., Ueno & Yasuda, 2003; Yasuda, 1997). Recent studies have shown strengthening ocean stratification in the subarctic North Pacific (Watanabe et al., 2001), which is expected to decrease both biological productivity and the ocean's capacity to buffer anthropogenic CO_2 (Doney et al., 2009; Intergovernmental Panel on Climate Change, 2013).

Therefore, we chose this region to test new parameterizations of oceanic carbon chemistry and their application to hydrographical data with high spatiotemporal resolutions obtained from Argo profiling floats. We used these reconstructed TA and DIC values along with oceanic carbon chemistry thermodynamics to calculate the quasi-real-time distribution of anthropogenic CO_2 (C_{ant}) at a high resolution in the subarctic North Pacific and examined the regional changes in C_{ant} over the last several decades.

2. Materials and Methods

2.1. Improved Parameterizations of TA and DIC in the Subarctic North Pacific

A previous study (Li et al., 2016) provided parameterizations for TA, DIC, and pH from 40- to 400-m depth in the subarctic North Pacific. By adding a pressure (*P*) parameter, we could provide new parameterizations for TA, DIC, and pH to 2000-m depth in the same region covering most of the subarctic North Pacific (40–56°N, 145°E-130°W, Figure S1). Because DO, *T*, *S*, and *P* have *F* values of more than 2.4 (Wilks, 2011, Tables 1 and S2), we can use the values of DO (μmol/kg), *T* (°C), *S* (dimensionless), and *P* (dbar) to reconstruct the predicted TA and DIC (TA_{pred} and DIC_{pred}; see equation S1 for pH):

$$TA_{pred} = 486.3 - 0.1031\ DO - 4.992\ T + 54.03\ S + 0.04155\ P \quad (1)$$

$$DIC_{pred} = 963.5 - 0.6485\ DO - 17.39\ T - 42.70\ S + 0.009313\ P \quad (2)$$

Equations (1) and (2) were obtained using the observed high-precision carbon chemistry and hydrographic data sets for DO, *T*, *S*, and *P* collected by the Climate Variability and predictability (available from the Carbon Dioxide Information Analysis Center: http://cdiac.ornl.gov/oceans) and Pacific Ocean Interior Carbon international programs from 2000 to 2010 (Suzuki et al., 2013). The data quality after 2000 were controlled by using Certified Referenced Materials distributed by A.G. Dickson of the Scripps Institution of Oceanography.

Table 1
Parameterizations for TA and DIC in the North Pacific subarctic region

	TA (n[a] = 3956)				DIC (n = 4004)			
	R^2 [b]	RMSE[c]	F[d]	VIF[e]	R^2	RMSE	F	VIF
DO[f]	0.98	8.18	1394	4.3	0.99	5.60	118721	4.2
T[g]			2762	2.0			72074	2.1
S[f]			5414	6.9			7228	6.9
P[g]			7935	4.0			855	4.0

Note. DIC = dissolved inorganic carbon; TA = total alkalinity.
[a]Number of data points. [b]Coefficient of determination. [c]Root-mean-square error. [d]Value from F test. [e]Variance inflation factor. VIF > 10 is a standard threshold for assessing collinearity (Kutner et al., 2004). [f]Value derived from the discrete Niskin bottles. [g]Value derived from the CTD sensor.

2.2. Application of Parameterizations and Argo-Based DO, *T*, and *S* Data to the Estimation of the C_{ant} and Disequilibrium DIC (C_{diseq})

According to Sarmiento and Gruber (2006), the sum of the anthropogenic DIC (C_{ant}) and disequilibrium DIC (C_{diseq}) can be calculated as C_{res} as follows:

$$C_{res} = C_{ant} + C_{diseq} = DIC - C_{pi,sat} - C_{soft} - C_{carb} \quad (3)$$

where $C_{pi,\,sat}$ (preindustrial saturated DIC) and C_{res} are preformed components, and C_{soft} (derived from the remineralization of organic matter) and C_{carb} (derived from the dissolution of $CaCO_3$, see below) are regenerated components. We used the predicted DIC (DIC_{pred}) calculated by equation (2) instead of the observed DIC. For the parameterization of DIC_{pred}, we used observed DIC data from the 2000s, which were influenced by a direct-anthropogenic component derived from the increasing level of anthropogenic CO_2 and an indirect-anthropogenic component derived from changes in DO, *T*, *S*, and *P*; thus, DIC_{pred} consists of C_{ant} from the 2000s and indirect-anthropogenic DIC at an arbitrary time. Here we assumed that the C_{ant} component of DIC_{pred} was constant at the C_{ant} value in 2005, determined by calculating the average C_{ant} value during 2000–2010.

$C_{pi,\,sat}$ can be calculated from the equilibrium carbon chemistry relationships as follows:

$$C_{pi,sat} = f\,(TA_0, pCO_2 = 280\ \text{ppm}, T, S, P) \quad (4)$$

where TA_0 is preformed TA from the sea surface obtained from the linear relationship between TA_0 and salinity ($TA_0 = 399 + 54.629S$, Millero et al., 1998). We calculated the contribution of organic matter remineralization to DIC as

$$C_{soft} = 117/170\ \text{AOU} \quad (5)$$

where 117/170 is the stoichiometric ratio of carbon to oxygen (Anderson & Sarmiento, 1994) and AOU is apparent oxygen utilization, calculated as the difference between saturated DO and observed DO. Here we assumed that the stoichiometric ratio was constant vertically and used the N: C: O_2 ratio of 16: 117: −170 (Anderson & Sarmiento, 1994). We calculated the contribution from the dissolution of $CaCO_3$ as

$$C_{carb} = 0.5\left(TA_{pred} - TA_0 - 16/170\ \text{AOU}\right) \quad (6)$$

where 16/170 is the stoichiometric ratio of nitrogen to oxygen (Anderson & Sarmiento, 1994). The term 16/170AOU corrects the calculation for the fact that TA also includes nitrate formed by the remineralization of organic matter. The coefficient 0.5 indicates that a change of one mole in TA corresponds to a change of one-half mole in DIC.

We did not use the traditional method to calculate the disequilibrium DIC in seawater (Gruber et al., 1996), because we did not have any seawater age information. Therefore, assuming that the CO_2 disequilibrium value would be constant from the surface mixed layer to the ocean interior, we estimated the CO_2 disequilibrium value at the mixed layer depth (MLD, $C_{diseq,\,MLD}$) by subtracting the preformed and regenerated

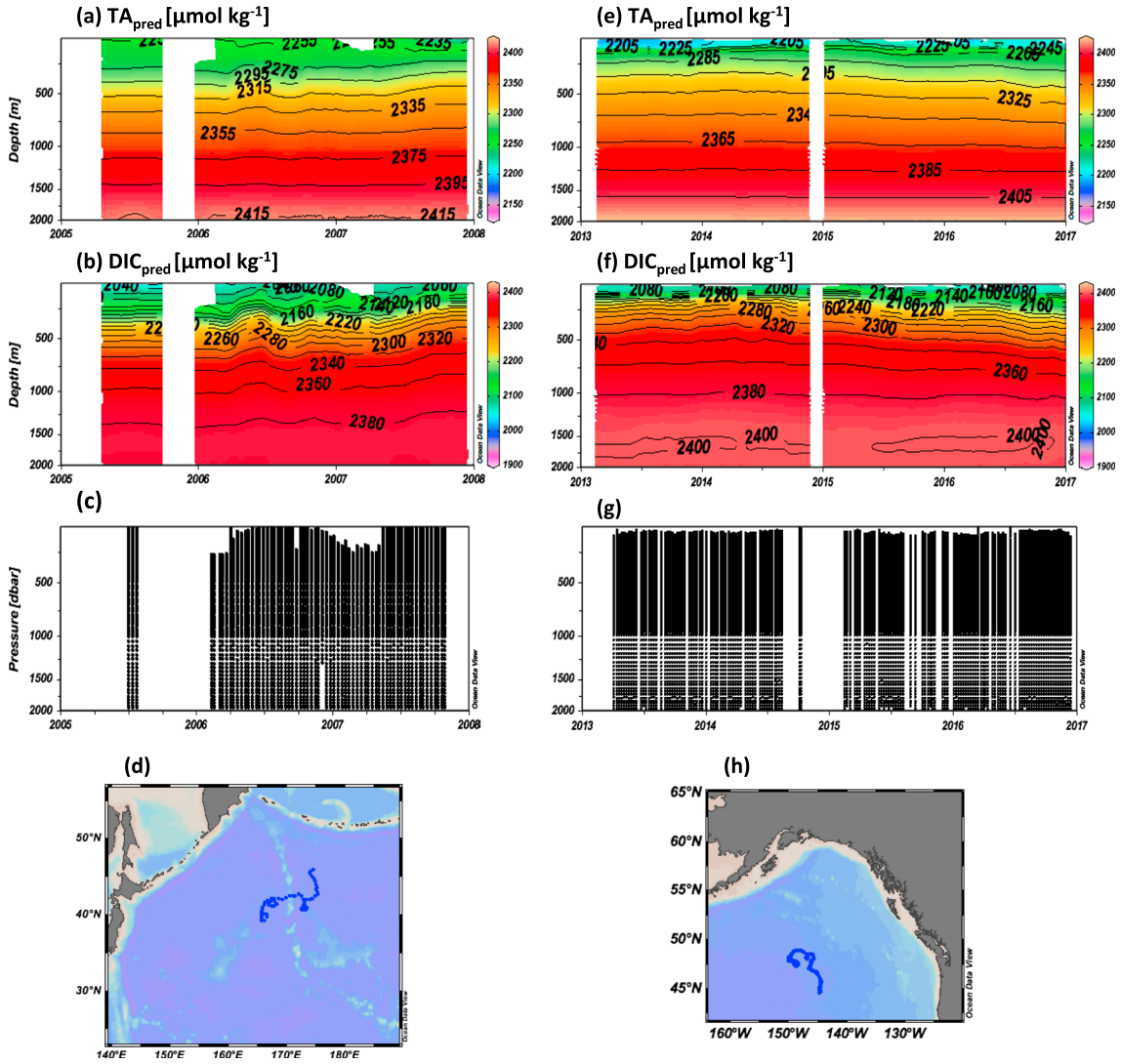

Figure 1. Vertical distributions of (a, e) TA_{pred} (μmol/kg) and (b, f) DIC_{pred} (μmol/kg) above 2,000-m depth predicted by applying new parameterizations to DO, *T*, and *S* data from Argo profiling floats 2900540 and 5904106, with (c, g) sampling profiles and (d, h) trajectory maps, respectively, drawn using Ocean Data View (http://odv.awi.de). DIC = dissolved inorganic carbon; TA = total alkalinity.

components at the MLD [saturated DIC at MLD ($C_{sat,\ MLD}$) and C_{soft} and C_{carb} at MLD ($C_{carb,MLD}$ and $C_{carb,\ MLD}$, respectively)] from DIC_{pred} at the MLD ($DIC_{pred\ MLD}$). Thus, $C_{diseq,\ MLD}$ in 2005 was calculated as

$$C_{sat,MLD} = f\ (TA_0, pCO_2 = 375\ \text{ppm}, T, S, P) \tag{7}$$

$$C_{diseq,MLD} = DIC_{pred,MLD} - C_{sat,MLD} - C_{soft,MLD} - C_{carb,MLD} \tag{8}$$

Because the DIC_{pred} value in 2005 included C_{ant}, we used 375 ppm as the pCO_2 value in 2005 in equation (7). We used the mean values of $C_{diseq,\ MLD}$ of each Argo float as C_{diseq} for all periods of that float. Finally, we estimated C_{ant} as

$$C_{ant} = C_{res} - C_{diseq} \tag{9}$$

3. Results and Discussion

By the 1990s, C_{ant} had penetrated as deep as ~1,500 m in the subarctic North Pacific (Sabine et al., 2004). This suggests that parameterizations of ocean carbon chemistry should be considered to 2,000-m depth (the

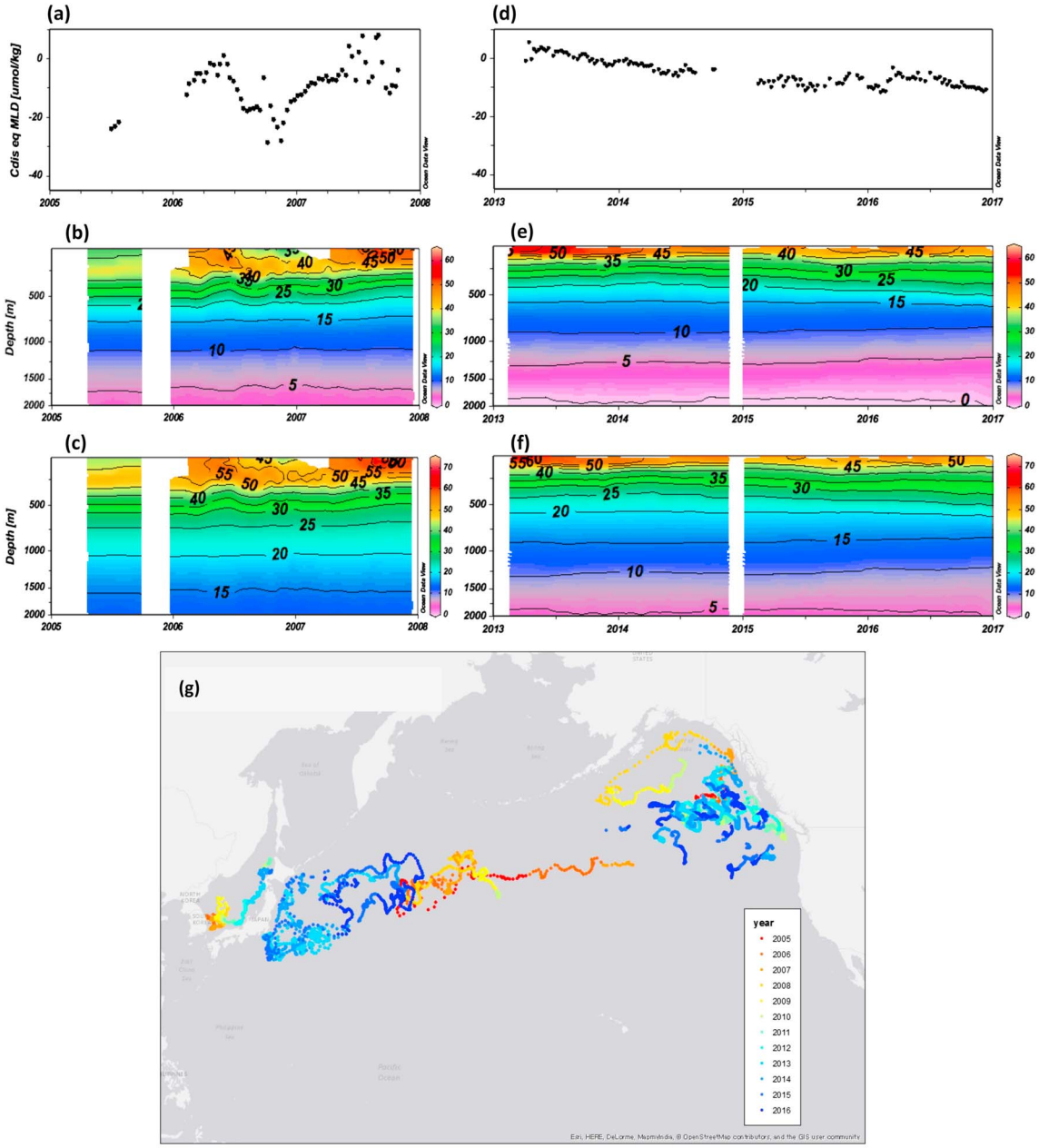

Figure 2. Vertical distributions of (a, d) $C_{diseq,\ MLD}$ (μmol/kg), (b, e) C_{res} (μmol/kg), and (c, f) C_{ant} (μmol/kg) predicted by applying new parameterizations to DO, *T*, and *S* data from Argo profiling floats 2900540 and 5904106, respectively. The vertical axis of (b, e, c, f) has been stretched at the top part of each panel. Figures 2a–2f were drawn using Ocean Data View (http://odv.awi.de). (g) BGC-Argo float trajectories in the subarctic North Pacific with trajectories in different years shown by colored dots. MLD = mixed layer depth; BGC-Argo = biogeochemical Argo float.

measurement limit for BCG-Argo floats) in this region to examine how the distribution of C_{ant} has changed. In addition, *P* is a main factor affecting the dissociation constants of carbonic acid and the dissolution of calcium carbonate in the ocean, so that we developed parameterizations of TA and DIC to 2,000-m depth that considered *P* (equations (1) and (2)).

For equation (1), the root-mean-square error (RMSE) was 8.2 μmol/kg and the coefficient of determination R^2 was 0.98; for equation (2), RMSE was 5.6 μmol/kg and R^2 was 0.99. These relationships were consistent

Table 2
Comparisons of C_{diseq} Between Sabine et al. (2002) and This Study

	Sabine et al. (2002)		This study	C_{diseq} (μmol kg^{-1})
	ID[b]	C_{diseq} (μmol kg^{-1})	C_{diseq} (μmol kg^{-1})	
West	1c	−4.85	−9.2	−4.35
	1e	−6.24		−2.96
	2a	−9.84		0.64
	3c	−2.52		−6.68
East	1c	−4.85	−5.1	−0.25
	1e	−6.24		1.14
	2a	−9.84		4.74
	3c	−2.52		−2.58

[a]Difference between C_{dis} calculated in this study and in Sabine et al. (2002). [b]Water types defined in Sabine et al. (2002): 1c, 33.2 < S < 33.75 and θ < 4; 1e, S < 33.65 and θ < 4.2; 2a, S < 33.94 and θ > 2.6; 3c, 33.2 < S < 34.5 and DO < 50 μmol/kg (θ = potential temperature in degree Celsius).

with their parameterizations to 400-m depth, used to reconstruct oceanic carbon chemistry at weekly to decadal scales (*Li* et al., 2016, sections S1 and S2 and Table 1). Combining these parameterizations with C_{ant} while only considering the RMSEs of TA_{pred} and DIC_{pred}, we calculated C_{ant}, the disequilibrium value of DIC (C_{diseq}), and their sum (C_{res}) with a precision of ±6.9 μmol/kg using DO, *T*, *S*, and *P* data over the subarctic North Pacific.

DO-Argo floats used in this study are mostly deployed in the western and eastern parts of the subarctic North Pacific. Although Argo DO data can be validated by comparison with discrete DO observation data obtained from bottle samples collected near the float locations, in this region such data are insufficient and too shallow to validate all DO-Argo data (Bushinsky et al., 2016). Therefore, we chose and tested two DO-Argo floats (WMO ID: 2900540 [west DO-Argo] and 5904106 [east DO-Argo], details in section S3) in the western and eastern gyres of the subarctic North Pacific. We then corrected the DO-Argo data using a linear fit to bottle DO data collected near each DO-Argo float (section S3 and Figure S5) and applied the new TA and DIC parameterizations to the DO, *T*, *S* and *P* of BGC-Argo data sets collected from the two gyres (Figure 1). The results showed that the vertical distributions of TA_{pred} and DIC_{pred} varied over a wider range and changed more smoothly in the east than in the west, mostly consistent with previous findings (Li et al., 2016).

We used the DIC_{pred} and TA_{pred} to calculate C_{ant}, C_{diseq}, and C_{res} using Argo DO, *T*, *S*, and *P* data over the subarctic North Pacific (Figure 2). Here C_{res} and C_{ant} represent the anthropogenic injection of CO_2 into the ocean until 2005 as an average from 2000 to 2010.

As we had no data on seawater age, we could not use the traditional method of estimating C_{diseq} due to disequilibrium in the air-sea exchange (Gruber et al., 1996). Instead, we assumed that the C_{diseq} would be constant vertically from the surface mixed layer and subtracted the preformed and regenerated components from DIC_{pred} at the mixed layer depth (MLD, $C_{diseq,\ MLD}$) as the C_{diseq} value. We used the mean $C_{diseq,\ MLD}$ value of each Argo float as C_{diseq} for all periods. The $C_{diseq,\ MLD}$ for west and east DO-Argo was −9.2 μmol/kg and − 5.1 μmol/kg, respectively (Figure 2), corresponding to the order of magnitude for C_{diseq} (−13 ± 5 μmol/kg) calculated by the traditional trace age method in a previous study of the North Atlantic (Gruber et al., 1996). We also compared our C_{diseq} to another C_{diseq} determined by the mixing of different water types (Sabine et al., 2002); the difference was less than 6 μmol/kg (Table 2).

Most $C_{diseq,\ MLD}$ values were negative because they represented an air-sea CO_2 exchange period of about 1/2 year (Figure 2). Some positive $C_{diseq,\ MLD}$ values appeared in the summer (April–June, Figures 2a and 2d) for both Argo floats. This result indicates that a shallower MLD may facilitate the air-sea exchange of CO_2, making it temporarily easier to reach equilibrium. As we found that C_{diseq} was not always constant in a given region and changes both seasonally and locally, our new method for estimating C_{diseq} without seawater age information is useful for C_{ant} calculation and can be broadly applied to Argo or other higher-resolution ocean hydrographic data in the future.

In the subarctic North Pacific, C_{ant} reached depths deeper than 1,700 m, about 300-m deeper than C_{ant} in the 1990s (Figure 2). C_{ant} penetrated more deeply in the west than in the east and was relatively high; this result was consistent with the isopycnal distribution of C_{ant} calculated by a previous global-scale study (Sabine et al., 2004). In addition, west DO-Argo drifted at relatively low latitudes and therefore had a lower buffering factor than east DO-Argo, which drifted at higher latitudes. The average C_{ant} inventories of west and east DO-Argo were 32.3 and 17.3 mol/m^2, respectively. The average inventory of C_{ant} in the subarctic North Pacific to 2,000-m depth was therefore 24.8 ± 10.2 mol/m^2, about 20% higher than the average during the 1990s (Sabine et al., 2004). The rate of ocean uptake of CO_2 was 0.5 mol·m^{-2}·year^{-1} in this region, a relatively low value for the North Pacific (Sabine et al., 2008). This low value may reflect a strengthening of ocean stratification in the subarctic North Pacific (Watanabe et al., 2001).

4. Conclusions

In this study, we showed the Lagrangian variations of carbon species and C_{ant} when using Argo data. Furthermore, we demonstrated that Argo floats in a specific region can be connected to produce time series data. Combining Argo data with our parameterizations allows the development of a system for monitoring long-term trend changes in ocean carbon chemistry similar to other time series stations (e.g., ALOHA and KNOT). Argo floats equipped with pH sensors in the subarctic North Pacific will inevitably be deployed in the near future. Since the pH sensors give us the high-resolution spatiotemporal distribution of ocean pH, we will easily use the sensor pH and our parameterized pH to separate the direct- and indirect-anthropogenic effect on ocean acidification in the future (Watanabe et al., 2018).

By using BGC-Argo or other automatic sensor data sets for DO, *T*, *S*, and *P*, our parameterizations can produce detailed spatiotemporal distributions of ocean carbon chemistry and anthropogenic CO_2 above 2,000-m depth in quasi-real time over the subarctic North Pacific, which traditional ship-based methods cannot achieve. In the future, application of our parameterization method to global BGC-Argo data should make it possible to obtain a high-resolution map and detailed time series distribution of global oceanic CO_2 cycle parameters.

Acknowledgments
We thank many scientists and technicians for their dedication in making long-term observations in the subarctic North Pacific region. We also extend our profound thanks for anonymous reviewers for their fruitful comments. This study was partly supported by KAKENHI grant 18H04131 from the Ministry of Education, Culture, Sports, Science and Technology of Japan. This study was also partly supported by the Sasakawa Scientific Research Grant from The Japan Science Society. We would like to thank Editage (www.editage.jp) for English language editing. Data used in this study are shown in supporting information Texts S1–S3. Supporting information accompanies this paper.

References

Alin, S. R., Feely, R. A., Dickson, A. G., Hernandez-Ayon, J. M., Juranek, L. W., Ohman, M. D., & Goericke, R. (2012). Robust empirical relationships for estimating the carbonate system in the southern California Current System and application to CalCOFI hydrographic cruise data (2005–2011). *Journal of Geophysical Research*, *117*, C05033. https://doi.org/10.1029/2011JC007511

Anderson, L. A., & Sarmiento, J. L. (1994). Redfield ratios of remineralization determined by nutrient data-analysis. *Global Biogeochemical Cycles*, *8*(1), 65–80. https://doi.org/10.1029/93GB03318

Bushinsky, S. M., Emerson, S. R., Riser, S. C., & Swift, D. D. (2016). Accurate oxygen measurements on modified Argo floats using in situ air calibrations. *Limnology and Oceanography: Methods*, *14*(8), 491–505. https://doi.org/10.1002/lom3.10107

Bushinsky, S. M., Gray, A. R., Johnson, K. S., & Sarmiento, J. L. (2017). Oxygen in the Southern Ocean from Argo floats: Determination of processes driving air-sea fluxes. *Journal of Geophysical Research: Oceans*, *22*, 8661–8682. https://doi.org/10.1002/2017JC012923

Carval, T., Keeley, R., Takatsuki, Y., Yoshida, T., Loch, S., Schmid, C., et al. (2017). *Argo user's manual*, *V3*, 2. https://doi.org/10.13155/29825

Doney, S. C., Balch, W. M., Fabry, V. J., & Feely, R. A. (2009). Ocean acidification: A critical emerging problem for the ocean sciences. *Oceanography*, *22*(4), 16–25. https://doi.org/10.5670/oceanog.2009.93

Gruber, N., Sarmiento, J. L., & Stocker, T. F. (1996). An improved method for detecting anthropogenic CO_2 in the oceans. *Global Biogeochemical Cycles*, *10*(4), 809–837. https://doi.org/10.1029/96GB01608

Inoue, R., & Kouketsu, S. (2015). Physical oceanographic conditions around the S1 mooring site. *Journal of Oceanography*, *72*(3), 453–464. https://doi.org/10.1007/s10872-015-0342-0

Intergovernmental Panel on Climate Change (2013). *Climate Change 2013: The Physical Science Basis. Contribution of Working Group I to the Fifth Assessment Report of the Intergovernmental Panel on Climate Change* (1535 pp.). Cambridge, UK and New York: Cambridge University Press. Retrieved from http://www.ipcc.ch/report/ar5/wg1/

Johnson, K. S., Plant, J. N., Coletti, L. J., Jannasch, H. W., Sakamoto, C. M., Riser, S. C., et al. (2017). Biogeochemical sensor performance in the SOCCOM profiling float array. *Journal of Geophysical Research: Oceans*, *122*, 6416–6436. https://doi.org/10.1002/2017JC012838

Juranek, L. W., Feely, R. A., Gilbert, D., Freeland, H., & Miller, L. A. (2011). Real-time estimation of pH and aragonite saturation state from Argo profiling floats: Prospects for an autonomous carbon observing strategy. *Geophysical Research Letters*, *38*, L17603. https://doi.org/10.1029/2011GL048580

Kutner, M., Nachtsheim, C., & Neter, J. (2004). *Applied linear regression models*. Boston, MA: McGraw-Hill.

Le Quere, C., Peters, G. P., Andres, R. J., Andrew, R. M., Boden, T. A., Ciais, P., et al. (2014). Global carbon budget 2013. *Earth System Science Data*, *6*(1), 235–263. https://doi.org/10.5194/essd-6-235-2014

Lee, K., Tong, L. T., Millero, F. J., Sabine, C. L., Dickson, A. G., Goyet, C., et al. (2006). Global relationships of total alkalinity with salinity and temperature in surface waters of the world's oceans. *Geophysical Research Letters*, *33*, L19605. https://doi.org/10.1029/2006GL027207

Li, B., Watanabe, Y. W., & Yamaguchi, A. (2016). Spatiotemporal distribution of seawater pH in the North Pacific subpolar region by using the parameterization technique. *Journal of Geophysical Research: Oceans*, *121*, 3435–3449. https://doi.org/10.1002/2015JC011615

Millero, F. J., Lee, K., & Roche, M. (1998). Distribution of alkalinity in the surface waters of the major oceans. *Marine Chemistry*, *60*(1–2), 111–130. https://doi.org/10.1016/S0304-4203(97)00084-4

Nakano, Y., & Watanabe, Y. W. (2005). Reconstruction of pH in the surface seawater over the north pacific basin for all seasons using temperature and chlorophyll-a. *Journal of Oceanography*, *61*(4), 673–680. https://doi.org/10.1007/s10872-005-0075-6

Riser, S. C., & Johnson, K. S. (2008). Net production of oxygen in the subtropical ocean. *Nature*, *451*(7176), 323–325. https://doi.org/10.1038/nature06441

Sabine, C. L., Feely, R. A., Gruber, N., Key, R. M., Lee, K., Bullister, J. L., et al. (2004). The oceanic sink for anthropogenic CO_2. *Science*, *305*(5682), 367–371. https://doi.org/10.1126/science.1097403

Sabine, C. L., Feely, R. A., Key, R. M., Bullister, J. L., Millero, F. J., Lee, K., et al. (2002). Distribution of anthropogenic CO_2 in the Pacific Ocean. *Global Biogeochemical Cycles*, *16*(4), 1083. https://doi.org/10.1029/2001GB001639

Sabine, C. L., Feely, R. A., Millero, F. J., Dickson, A. G., Langdon, C., Mecking, S., & Greeley, D. (2008). Decadal changes in Pacific carbon. *Journal of Geophysical Research*, *113*, C07021. https://doi.org/10.1029/2007JC004577

Sarmiento, J. L., & Gruber, N. (2006). *Ocean biogeochemical dynamics*. Princeton University Press.
Suzuki, T., Ishii, M., Christian, J., & Kozyr, A. (2013). PACIFICA data synthesis project. ORNL/CDIAC-159 NDP-092, Carbon Dioxide Information Analysis Center, Oak Ridge National Laboratory, U.S. Department of Energy, Oak Ridge, TN.
Takeshita, Y., Martz, T. R., Johnson, K. S., Plant, J. N., Gilbert, D., Riser, S. C., et al. (2013). A climatology-based quality control procedure for profiling float oxygen data. *Journal of Geophysical Research: Oceans*, *118*, 5640–5650. https://doi.org/10.1002/jgrc.20399
Thierry, V., & Bittig, H. (2016). Argo quality control manual for dissolved oxygen concentration. Argo-BGC group. DOI: https://doi.org/10.13155/46542
Ueno, H., & Yasuda, I. (2003). Intermediate water circulation in the North Pacific subarctic and northern subtropical regions. *Journal of Geophysical Research*, *108*(C11), 3348. https://doi.org/10.1029/2002JC001372
Watanabe, Y. W., Li, B. F., & Wakita, M. (2018). Long-term trends of direct and indirect anthropogenic effects on changes in ocean pH. *Geophysical Research Letters*, *45*, 9106–9133. https://doi.org/10.1029/2018GL078084
Watanabe, Y. W., Ono, T., Shimamoto, A., Sugimoto, T., Wakita, M., & Watanabe, S. (2001). Probability of a reduction in the formation rate of the subsurface water in the North Pacific during the 1980s and 1990s. *Geophysical Research Letters*, *28*(17), 3289–3292. https://doi.org/10.1029/2001GL013212
Wilks, D. S. (2011). *Statistical methods in the atmospheric sciences*. United States: Academic Press.
Williams, N. L., Feely, R. A., Sabine, C. L., Dickson, A. G., Swift, J. H., Talley, L. D., & Russell, J. L. (2015). Quantifying anthropogenic carbon inventory changes in the Pacific sector of the Southern Ocean. *Marine Chemistry*, *174*, 147–160. https://doi.org/10.1016/j.marchem.2015.06.015
Williams, N. L., Juranek, L. W., Johnson, K. S., Feely, R. A., Riser, S. C., Talley, L. D., et al. (2016). Empirical algorithms to estimate water column pH in the Southern Ocean. *Geophysical Research Letters*, *43*, 3415–3422. https://doi.org/10.1002/2016GL068539
Yasuda, I. (1997). The origin of the North Pacific intermediate water. *Journal of Geophysical Research*, *102*(C1), 893–909. https://doi.org/10.1029/96JC02938